

# Instrumentation for high-resolution spectropolarimetry in the visible and far-ultraviolet.

Kenneth H. Nordsieck, Kurt P. Jaehnig, Eric B. Burgh, Henry A. Kobulnicky, Jeffrey W. Percival,  
Michael P. Smith

Space Astronomy Laboratory, University of Wisconsin, Madison, WI 53706

## ABSTRACT

Linear spectropolarimetry of spectral lines is a neglected field in astronomy, largely because of the lack of instrumentation. Techniques that have been applied, but rarely, include investigation of the dynamics of scattering envelopes through the polarization of electron- or dust-scattered nebular light. Untried techniques include promising new magnetic diagnostics like the Hanle Effect in the far-ultraviolet and magnetic realignment in the visible. The University of Wisconsin Space Astronomy Lab is developing instrumentation for such investigations. In the visible, the Prime Focus Imaging Spectrograph (PFIS) is a first light instrument for the Southern African Large Telescope (SALT), which at an aperture of 11m will be the largest single telescope in the Southern Hemisphere. Scheduled for commissioning in late 2004, PFIS is a versatile high-throughput imaging spectrograph using volume-phase holographic gratings for spectroscopic programs from 320nm to 900nm at resolutions of  $R=500$  to  $R=6000$ . A dual-etalon Fabry-Perot subsystem enables imaging spectroscopy at  $R=500$  and  $R=3000$  or 12,500. The polarization subsystem, consisting of a very large calcite polarizing beam-splitter used in conjunction with half- and quarter-wave Pancharatnam superachromatic plates, allow linear or circular polarimetric measurements in any of the spectroscopic modes. In the FUV, the Far-Ultraviolet SpectroPolarimeter (FUSP) is a sounding rocket payload, scheduled for its first flight in 2003, that will obtain the first high-precision spectropolarimetry from 105 – 150 nm, and the first astronomical polarimetry of any kind below 130 nm. The 50 cm primary mirror of the telescope is F/2.5. At the prime focus are the polarimetric optics, a stressed lithium fluoride rotating waveplate, followed by a synthetic diamond Brewster-angle mirror. The spectrometer uses an aberration-corrected spherical holographic grating and a UV-sensitized CCD detector, for a spectral resolution of  $R=1800$ .

**Keywords:** linear spectropolarimetry, volume-phase holographic gratings, Fabry-Perot spectroscopy, waveplates, ultraviolet polarimetry, brewster polarizers

## 1. INTRODUCTION

Spectropolarimetry of astronomical objects beyond the Sun is still largely confined to relatively low spectral resolution ( $R = 500 - 2000$ ). Studies of polarimetric line profiles are rare except for greatly doppler-broadened lines like QSOs and bright supernovae. The prime reason is mainly photon statistics – strong lines are required to obtain adequate polarimetric precision, and going to high spectral resolution rapidly uses up precious photons. But a second obstacle has been the limited number of reliably interesting line effects so far seen, at least for the strong lines we can observe. We believe that new instrumentation is required to explore this territory, in which a large number of interesting effects have yet to be exploited. Some of these effects are:

- Three-dimensional "polarimetric tomography" through the observation of unpolarized lines scattered by a dynamic envelope of dust or electrons. Classic examples of such studies are M82<sup>1</sup> and  $\eta$  Car<sup>2</sup>, which use painfully compiled polarimetric profiles of strong lines as a function of position in a nebula. A wide-field high resolution spectropolarimeter would greatly aid such studies.
- Magnetic fields through the linear polarization of resonance lines<sup>3</sup>. One such effect, the "Hanle Effect", has been used for the Sun but never beyond. It is sensitive to fields down to 1 G, but the strongest applicable lines (CIV, NV, SiIV) are in the ultraviolet – this awaits a UV spectropolarimeter. A related effect, "magnetic realignment", is sensitive to  $\mu$ G fields and works on visible lines like NaD, but the expected applications are for faint nebulae requiring a large telescope and an

imaging spectropolarimeter.

This paper describes two instruments now being built that are designed to explore this new territory.

## 2. SALT IMAGING SPECTROPOLARIMETER

### 2.1 Summary

The Southern African Large Telescope (SALT)<sup>4,5</sup> is an 11m telescope based on the Hobby-Eberly Telescope<sup>6</sup> concept, where a segmented spherical primary mirror is at a fixed elevation and celestial objects are tracked by moving the prime focus platform. The Prime Focus Imaging Spectrograph (PFIS) will be the major instrument at the prime focus. The PFIS optical system (Figure 1) consists of a collimator that accommodates an 8 arcmin diameter F/4.2 beam over the wavelength range 320 nm – 1.7  $\mu$ m. The 150 mm diameter collimated beam contains either Fabry-Perot etalons or a Volume Phase Holographic (VPH) transmission grating. When using the VPH gratings the camera is articulated around the grating axis to take advantage of the tunable blaze of the grating. The visible wavelength camera focuses the wavelength range 320 – 900 nm at F/2.2 onto a focal plane array of three 4096 x 2048 CCD's. Provision is made for a future simultaneous Near InfraRed (NIR) beam, using a chromatic beam-splitter before the last doublet of the collimator, a NIR collimator doublet, and a NIR camera. A more detailed description of the PFIS optical design is given elsewhere<sup>7</sup>.

The polarimetric module consists of two superachromatic waveplates, half- and quarter-wave, inserted in the diverging beam within the collimator, and an array of calcite Wollaston beamsplitters inserted in the visible wavelength collimated beam. Waveplates and beamsplitter may be removed for non-polarimetric operations. PFIS will specialize in very high throughput, low- and medium-resolution ( $R = 500 - 12000$ ) spectroscopy and spectropolarimetry from 320 to 900 nm, using either the VPH gratings or the double etalon Fabry-Perot system<sup>8</sup>. With a spectrograph/ detector peak efficiency of 62% and a 320 nm efficiency above 25%, it will provide extremely high sensitivity spectropolarimetry in all of its modes. These modes intersect with polarimetry in interesting ways. For instance, UV spectropolarimetry provides access to crucial astrophysical features, such as CaII H,K, [OII]  $\lambda$ 3727, the Balmer Jump, Bowen lines in high excitation objects (OIII  $\lambda$ 3133, 3343, 3444), processed material lines in objects like novae ([NeV]  $\lambda$ 3340, 3425), and the strongest line in comets following Ly $\alpha$ : OH  $\lambda$ 3090. It is also important to realize that these wavelengths provide the lowest-redshift ground-based access to redshifted vacuum UV features like MgII  $\lambda$ 2800 (for  $z = 0.1 - 0.4$ ), the  $\lambda$ 2200 Bump ( $z = 0.4 - 0.8$ ), and Ly $\alpha$  ( $z = 1.6 - 2.3$ ). Next, medium resolution spectropolarimetry (both grating and Fabry-Perot) on a large telescope will for the first time provide useful polarimetric line profiles. Finally, the

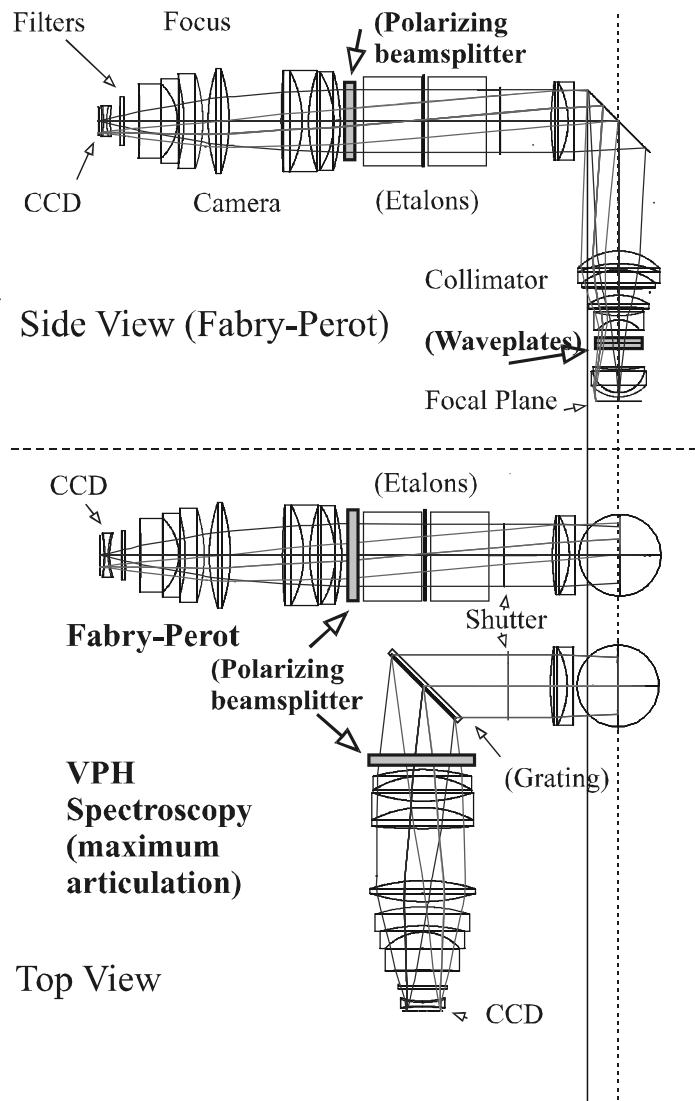


Figure 1. SALT/PFIS Optics. ( ) - removable

availability of multiobject spectropolarimetry will enable unique spectropolarimetric surveys of crowded regions available to SALT, like the Galactic plane and the Magellanic Clouds. Provision is made for a future IR beam (0.85 – 1.7 $\mu$ ), which would carry the PFIS capabilities into a new regime and allow unique simultaneous visible-IR spectropolarimetry.

## 2.2 Polarimeter Optical Design

Modern spectropolarimeters consist of two elements, a polarization modulator, which modulates the polarization state of the beam in time, and a polarization analyzer, which defines which polarization state is passed to the detector. Often the analyzer is a polarizing beam-splitter whose two output beams are detected simultaneously and the polarization signal is recovered from the modulation of the difference in intensity in the two beams. Beam-splitters allow the highest polarimetric precision because variations in atmospheric transparency and in the optics are cancelled out in the differential measurement. The placement of the beam-splitter often defines the field of view: in systems like the Keck LRIS spectropolarimeter<sup>9</sup>, the beam-splitter is a prism placed in the diverging beam just after the focal plane, with a thin-film interface that passes one sense of polarization and reflects the other, leading to two parallel beams displaced by a small amount perpendicular to the spectral dispersion. Because of the small displacement and the length of such prisms, the field of view cannot be very large, and these are generally used for stellar or compact objects. The other choice is to place a birefringent beamsplitter in the collimated beam, which causes the two orthogonally polarized beams to diverge perpendicular to the spectral dispersion; the spectrograph camera focuses the two beams into displaced spectra. The latter has been chosen for PFIS because of the desire to make use of the large field of view of the SALT telescope for multi-object spectropolarimetry and spectropolarimetric imaging of diffuse objects, both with the VPH grating, and, uniquely, the Fabry-Perot etalons. The prism is a Wollaston prism, which deviates the two beams equally by an amount that is proportional to the tangent of the prism interface angle, and thus the prism thickness.

The second choice that must be made is the nature of the polarizing prism. In the VLT FORS1 spectropolarimeter<sup>10</sup>, it is a very large (a 120 mm cube) crystal quartz Wollaston prism (prism angle 45°). This has the advantage that crystal quartz is very transparent, so that it has good throughput. The disadvantage is that the birefringence of this material is so small that even with such a thick prism, the deviation is much smaller than the field diameter. In FORS1, spectropolarimetry requires a "Venetian blind" slitmask that provides a shadow for each 22 arcsec slot to be doubled into two images. This is inefficient because the slot filling factor must be less than 1/2 to prevent beam overlap. Such a very large piece of quartz is also extremely expensive because it is too large to be grown synthetically – a natural piece of very high quality must be found. PFIS has chosen the other possibility, a thin calcite prism. Calcite has a very large birefringence, so that a modest prism angle serves to split the field of view into two completely separate halves. The PFIS prism, with an angle of 14.3°, splits a 4 $\times$ 8 arcmin field into two oppositely polarized fields separated by 4 arcmin perpendicular to the spectral dispersion. The disadvantage of calcite is that it is only available naturally, in rather small pieces that are not as transparent as quartz. For PFIS, the calcite prism is a mosaic of nine prisms, each one of which is 1/3 the aperture and thickness of a monolith. The increased efficiency of the use of the field of view is balanced by the decreased throughput of the calcite and the mosaic, so the two choices have similar throughput. Overall, the calcite solution has a more convenient use of the field of view, is much thinner so that it uses much less collimated beam, and is cheaper.

Another factor to be considered for the beamsplitter is that no birefringent material has a wavelength-independent birefringence – the splitting is wavelength dependent, so that every point source is actually split into two oppositely-directed spectra. This is not a large effect for the FORS1 quartz prism, because the splitting is not large, but it is an important effect for calcite. For PFIS, this dispersion is (figure 2) 25 arcsec from 320 to 900 nm. This rules out broadband polarimetric imaging of diffuse objects, especially in the blue, where the dispersion is largest. Since PFIS is specializing in spectroscopy, this is not judged to be a serious disadvantage. It also can be used to advantage, since without any dispersors in the beam, the polarizing prism provides enough spectral dispersion on

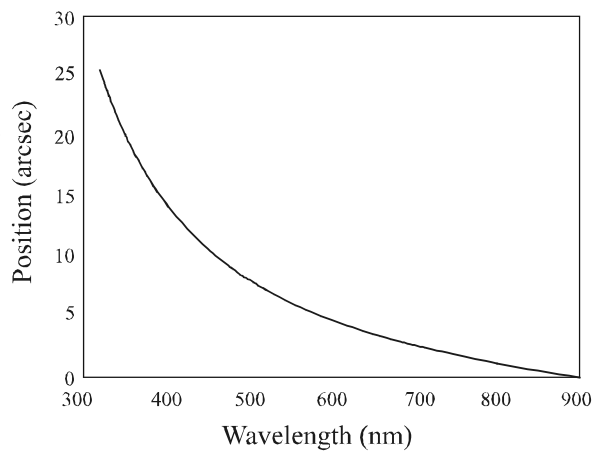


Figure 2. Beamsplitter chromatic dispersion

its own to create a unique very low resolution spectropolarimetric imaging mode allowing simultaneous spectropolarimetry of hundreds of faint objects.

The PFIS modulator is a rotating superachromatic waveplate near the beam waist in the collimator. Both half- and quarter-wave plates may be inserted. The half-wave plate accepts the full 105 mm beam, providing a field of view of 4×8 arcmin for linear spectropolarimetry. It is a mosaic of four 52 mm plates. The quarter-wave plate is a single 60mm element, providing a field of view of 3.9×4 arcmin for circular or all-Stokes spectropolarimetry.

### 2.3 Performance

Three other 8–10m telescopes have spectropolarimetric capability. Table 1 below compares their capabilities with the projected capability of the PFIS spectropolarimeter.

**Table 1.** Comparison of large telescope spectropolarimeters

Telescope	Instrument	FOV (arcmin)	Resolution $\lambda/\Delta\lambda$	Wavelength (nm)	Efficiency @ 360nm
Keck II	LRIS R,B <sup>9</sup>	0.4 dia	500 – 2000	310 – 1000	0.5
Subaru	FOCAS <sup>11</sup>	6×3	500 – 3000	365 – 900	0.13
VLT	FORS1 <sup>10</sup>	7×3.5	200 – 1800	360 – 1100	0
SALT	PFIS	8×4	500 – 6500	320 – 900	0.43

PFIS will have comparable UV throughput to Keck/ LRIS-B, with a much larger field. Of the wide -field spectropolarimeters, PFIS will be the only one with good UV throughput. The FOV will be the largest available, and the spectral resolution at least twice as big as the next largest. In addition, the Fabry-Perot imaging spectropolarimetry will be unique. The future capability for simultaneous visible/ NIR spectropolarimetry will also be unique.

For spectropolarimetry, we predict 0.3% accuracy per resolution element at 550 nm for a  $V = 18.5$  star at resolution  $R = \lambda/\Delta\lambda = 1500$ , and for the very low resolution mode ( $R = 20$ ) for a  $V = 20.7$  star.

### 2.4 Operational Modes

The waveplate modulators are to be used in three modes, linear, circular, and "all-Stokes" mode. For ease of operation, the waveplates are in the same order in all modes, half-wave first. Table 1 gives the waveplate angle progression for each mode. The angle shown is that between the waveplate optic axis and the beam-splitter polarization axis, which is 45° to the dispersion direction, as described below.

**Table 2.** Waveplate positions

Linear		Circular		All-Stokes	
1/2 $\lambda$	1/4 $\lambda$	1/2 $\lambda$	1/4 $\lambda$	1/2 $\lambda$	1/4 $\lambda$
0	-	0	+45	0	0
45	-	0	-45	22.5	33.75
22.5	-	22.5	-45	45	67.5
67.5	-	22.5	+45	67.5	101.25
11.25	-	45	+45	90	135
56.25	-	45	-45	112.5	168.75
33.75	-	67.5	-45	135	202.5
78.75	-	67.5	+45	147.5	236.25

Linear polarization mode uses just the half-wave plate in a standard sequence, with exposure pairs corresponding to  $90^\circ$  polarization position angle rotations (half-wave plate rotated  $45^\circ$ ). The first four positions are sufficient to determine the two linear polarization Stokes parameters, and could be used for faint objects where there may not be time for eight exposures. The remaining four positions give a redundant estimate of the Stokes parameters, which is useful for estimating systematic error for high precision work.

In circular polarization mode, both waveplates are used: the quarter-wave plate is alternated between the plus and minus 45 degree position, which converts circular polarization into linear polarization aligned and orthogonal to the beam-splitter polarization axis. The half-wave plate is used to rotate the axis of the incoming linear polarization to different angles to cancel out the effects of linear to circular conversion in the waveplates. This technique is used in all high precision circular polarimeters to measure small polarization ellipticities (small circular in the presence of large linear polarization) such as are typical in interstellar polarization and dust scattering nebulae. The linear to circular conversion in the optics before the modulator will be calibrated using objects of known polarization.

In "all-Stokes" mode, both waveplates are advanced with constant angular steps, causing the linear and circular polarization to modulate the intensities at the detector with differing frequencies. This would be used for objects with comparable linear and circular polarization (e.g. magnetic CVs), and especially for high time resolution sampling. The original all-Stokes mode suggested by Serkowski<sup>12</sup> uses a quarter-wave plate followed by a half-wave plate, each rotating at the same rate in opposite directions. The linear polarization signal appears at a frequency of twice and four times the rotation rate, and the circular polarization signal appears at three times the rotation rate. This is not suitable here, because the quarter-wave plate is first. We have found an alternate all-Stokes mode in which the half-wave plate is first, and the quarter-wave plate rotates at  $3/2$  the half-wave rate in the same direction. This results in the same frequency pattern and efficiency as the Serkowski method.

The maximum speed for any of these modes will be attained with a "shuffle-and-read" method of detector readout. A single star window is placed at the far end of the slit, with the rest of the slit masked. Each exposure is followed by a waveplate advance and a shuffle of the CCD to put the spectrum in an unexposed part of the detector. When the E and O part of the detector is full, the shutter must be closed and the CCD read out. Frame transfer is not possible in polarimetric modes because the E and O beams occupy the "image" and "storage" halves of the CCD simultaneously. The maximum rate will be set by the waveplate speed, not the detector. The current specification is for a  $90^\circ$  rotation in 2 seconds. In all-Stokes mode, the quarter-wave plate is stepped  $3/8$  of this, taking 0.75 seconds. If the lost duty cycle due to rotation is to be less than 10%, the minimum sample time is 7.5 sec, and eight samples to get the stokes parameters will require 60 seconds.

### 2.5 SALT Telescope Instrumental Polarization

One concern for precision spectropolarimetry is the instrumental linear polarization arising in the telescope itself. This is particularly so for SALT, where the very fast primary mirror and spherical aberration corrector result in large angles of incidence, and where vignetting in the SAC and by the primary mirror during

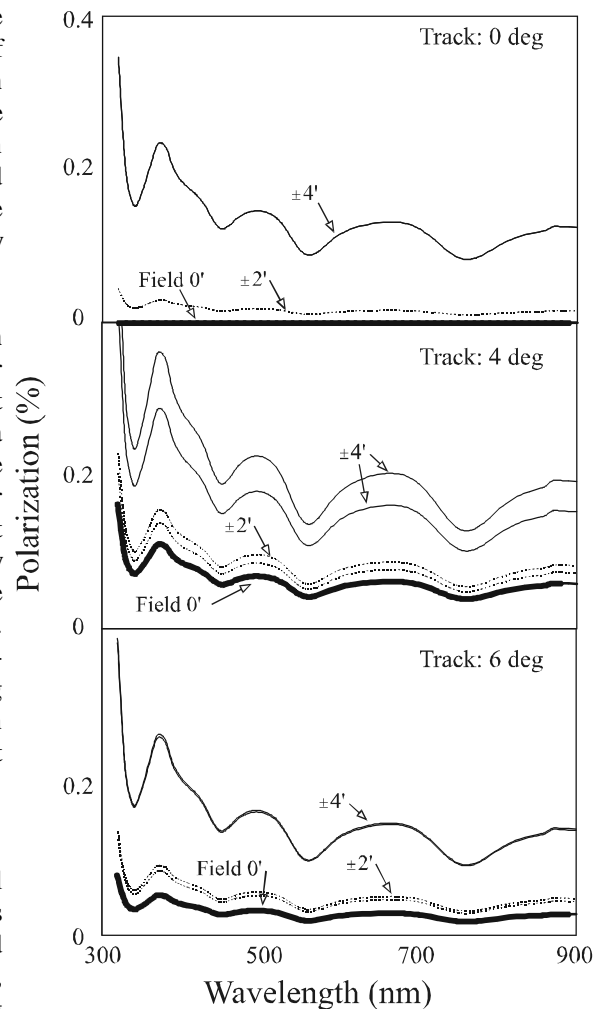


Figure 3. SALT instrumental polarization

a track causes an asymmetric pupil illumination for large field angles and large track angles. If this effect is to be calibrated, the magnitude of the effect must not be too large. Experience with other spectropolarimeter systems indicates that a residual systematic error of as much as 10% of the instrumental polarization correction can remain after calibration.

We have evaluated the expected instrumental polarization of the SALT telescope and SAC as a function of wavelength, field angle, and track angle, assuming an aluminum coated primary and all four SAC mirrors coated with the LLNL enhanced silver/ aluminum multilayer coating<sup>13</sup>. The LLNL group kindly provided us with the polarization as a function of angle and wavelength from a theoretical model of the coating. In order to put this into ZEMAX, the angular polarization behavior  $p(\theta)$  was found to be well represented by a single coating with the index of refraction  $n$  and  $k$  of an ideal metal (index  $k \gg n$ ):  $p(\theta) \sim 2 \sin \theta \tan \theta n/k^2$ . Based on this, the LLNL coating actually has a lower polarization than either aluminum or silver alone, except at the shortest wavelengths. Figure 3 illustrates the predicted instrumental polarization spectrum for the SALT telescope for several field angles and track angles. In these plots the field angle is in the same plane as the track angle, which is the worst case. The instrumental polarization is less than 0.1% for field angles less than 2 arcmin, and typically 0.2% for the largest field angles. The largest value is less than 0.4%. Based on the above rule of thumb, we should be able to reliably calibrate to better than  $\pm 0.04\%$ . The effect of the track angle is about 0.1%, smaller than the field angle effect, so that modeling the time-dependent polarization due to the track should not be difficult. We plan to use an empirical instrumental polarization model based on these calculations, with adjustable coefficients calibrated using unpolarized stars.

## 2.6 Waveplates

The waveplates are to be Pancharatnam "superachromatic" retarders. A single retardation plate is half- or quarter-wave at only one wavelength, mainly because the birefringence in microns, not wavelengths, is approximately wavelength independent. In a conventional achromatic waveplate, two different materials of different birefringence wavelength dependence (usually magnesium fluoride and crystal quartz) are crossed to produce a retarder that has some specified retardation at two wavelengths. In a Pancharatnam design<sup>14</sup>, two identical retarders surround a third retarder rotated by some angle; the parameters of this arrangement can also be chosen so that the combination has a specified retardation for at least two wavelengths. A Pancharatnam "superachromatic" retarder combines these techniques: each of the three Pancharatnam retarders is an achromatic pair of very thin (150 – 500 micron) plates of MgF<sub>2</sub> and crystal quartz, yielding a retarder that is close to the desired retardation over the entire visible band. Because of the thinness of the six elements, the aperture of the plate is limited, and large aperture plates must be fabricated as a mosaic (VLT FORS1 has a 100mm mosaic superachromatic plate). A waveplate covering the entire PFIS visible/ NIR wavelength range, 320 nm – 1.7 $\mu$ m, is readily designed, so that a single waveplate would serve both beams.

A complication is the fast F-ratio of the beam where the waveplates are inserted. The Pancharatnam design is relatively insensitive to incidence angles, but for the PFIS beam, serious effects are seen in the UV with a waveplate designed for a

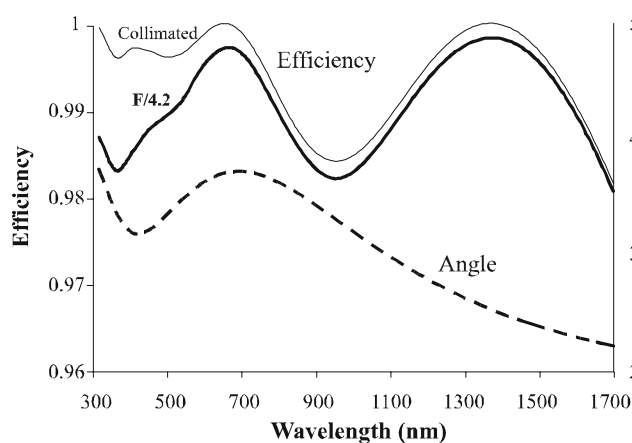


Figure 4. Half-wave Plate Performance

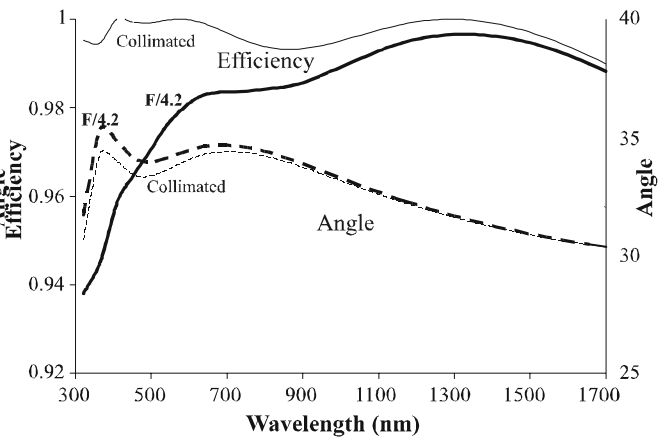


Figure 5. Quarter-wave Plate Performance

collimated beam. These effects manifest themselves in a reduced effective polarimetric efficiency, and in sensitivity to an asymmetrically illuminated pupil – a definite concern for SALT. We have designed Pancharatnam plates specifically for the PFIS beam (figure 4,5). The efficiency reduction due to the fast beam is small for the half-wave plate. For the quarter-wave plate, the design is constrained by the minimum achievable thickness for the individual plates, 250  $\mu\text{m}$ , leading to a larger, but still acceptable, effect.

### 2.7 Beamsplitter

The polarization analyzer will be a mosaic of calcite Wollaston beamsplitters (figure 6). The polarimetric field (masked to a 4x8 arcmin rectangle) is split into two fields (Ordinary and Extraordinary) separated by 4 arcmin perpendicular to the spectral dispersion, filling the CCD. The polarization position angle of the E and O beam is chosen to be  $\pm 45^\circ$  from the dispersion axis, so that the throughput of the two beams are matched in spite of the polarization sensitivity of the fold mirror and the grating. In grating spectroscopy mode, every spectrum is split into an E and an O spectrum. Since the beam splitting is wavelength dependent, the spectra are slightly curved. In Fabry-Perot mode, the image appears twice, separated by the splitting at the selected Fabry-Perot wavelength. Without a dispersor, two images are seen, with each point object stretched into a prism-dispersion spectrum perpendicular to the usual spectral dispersion, leading to the aforementioned very low resolution spectropolarimetric imaging mode.

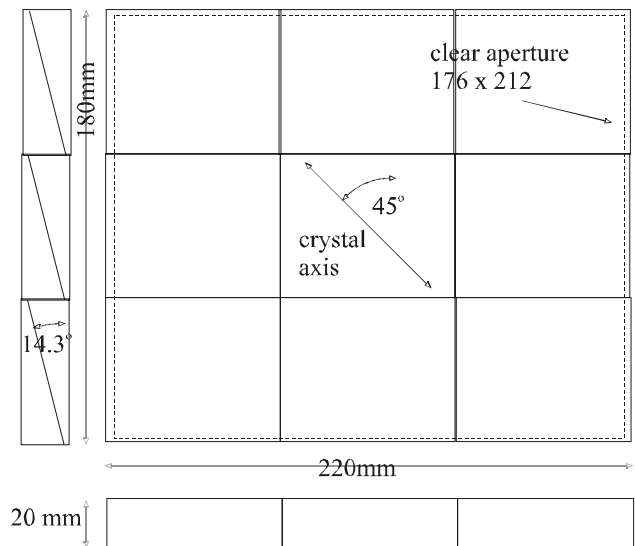


Figure 6. SALT PFIS Polarizing Beamsplitter

## 3. FAR-ULTRAVIOLET SPECTROPOLARIMETER (FUSP)

### 3.1 Science Overview

A major goal of modern astrophysics is determining how mass and energy circulate between stars and the interstellar medium. This crucial process takes place in the circumstellar environment. The available evidence indicates that neither the physics nor the geometry of this process is simple, and that angular momentum and magnetic fields are fundamentally important. The objective of FUSP is to test potentially powerful new diagnostics of the dynamics, geometry, and magnetic field of envelopes of hot objects using spectropolarimetry in the Far Ultraviolet. These tools will be applied to the fundamental question:

*Under what circumstances and how do angular momentum and magnetic fields control accretion and mass outflow in compact objects?*

FUSP is a sounding rocket payload that will obtain high precision spectropolarimetry from 105 – 150 nm for hot stellar sources, making use of the increased importance of polarizing opacities in the FUV (figure 7). It will measure the polarization produced by electron scattering, resonance line scattering, and hydrogen Rayleigh scattering in the inner circumstellar environment, and thereby quantitatively constrain the geometry and dynamics of the system. The strength and geometry of the magnetic field will be

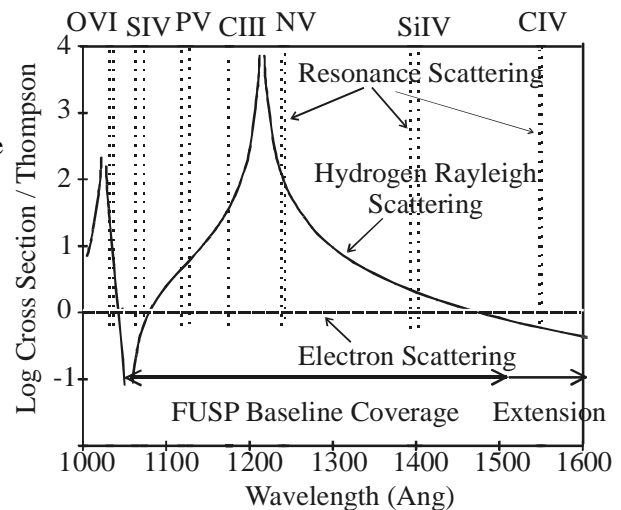


Figure 7. Far UV Polarizing Opacities

determined from the polarization of resonance scattering through the Hanle Effect.

### 3.2 Instrument Design

To the best of our knowledge, useful astronomical polarimetric data in the Far Ultraviolet (91 –135 nm) have never been obtained. A major technical obstacle has been the lack high-efficiency polarimetric optics. We have now devised a highly efficient polarimetric modulator/ analyzer that works down to 105 nm. Two practical astronomical factors suggest incorporation of these elements into a spectropolarimeter (rather than low-resolution polarimeter): the ubiquity of strong astrophysical absorption and emission lines in this region, which appear to be important in polarizing stellar envelopes, and the presence of strong airglow and geocoronal lines that must be removed for useful faint-object work.

Figure 8 illustrates the FUSP optical section. The telescope is a simple 50 cm F/2.5 parabola: the aperture is the largest that will fit in a 22 inch (bulbous) rocket skin, and the focal ratio is the fastest that may be accommodated by the spectropolarimeter. The primary mirror is cut down to 35 cm (F/3.5) in the direction of the spectral dispersion to allow for support structure and to minimize steep reflections in the spectrometer. At the prime focus is mounted the spectropolarimeter (Figure 9), a sealable housing with the polarimetric elements, grating, and detector. The detector is a thinned, overcoated 1024×1024 SITe

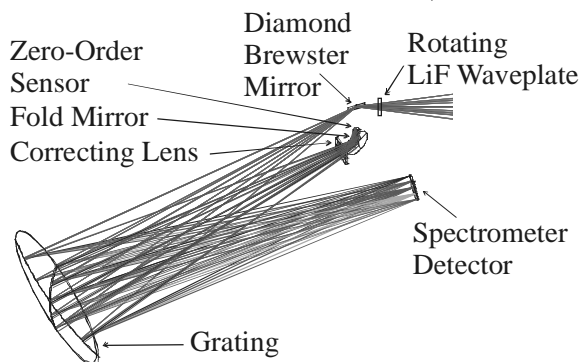


Figure 9 FUSP Spectropolarimeter

CCD, cooled to about -65 °C by a Thermo-Electric Cooler. The primary mirror and spectrometer coatings will be LiF overcoated Aluminum. The entire telescope section may be evacuated or backfilled with dry nitrogen, with the aperture sealed by a NASA standard vacuum door. This is desirable in order to preserve the delicate LiF coatings and to provide an FUV liveness test in the field.

The polarimetric modulator is a 12 mm square, 1 mm thick stressed-LiF waveplate, mounted just before the focus. The waveplate is made to be half-wave at 124 nm by applying about 15 pounds pressure to one edge of the plate; polarimetric modulation is performed by rotating the plate 45°, which rotates the plane of polarization by 90°. The LiF plate is the only transmissive element in the instrument, and results in a short wavelength limit of 105 nm. Stressed-LiF waveplates have been used in the past for laboratory work at Ly  $\alpha$ <sup>15</sup>. The piezo-birefringence of LiF has been measured down to 120 nm<sup>16</sup>; it increases rapidly as one approaches the UV absorption edge at 105 nm, which will limit the useful simultaneous bandwidth to 50 nm.

The polarization analyzer is a 10 mm square diamond mirror mounted at the telescope prime focus at an angle of 72.5°, near the Brewster

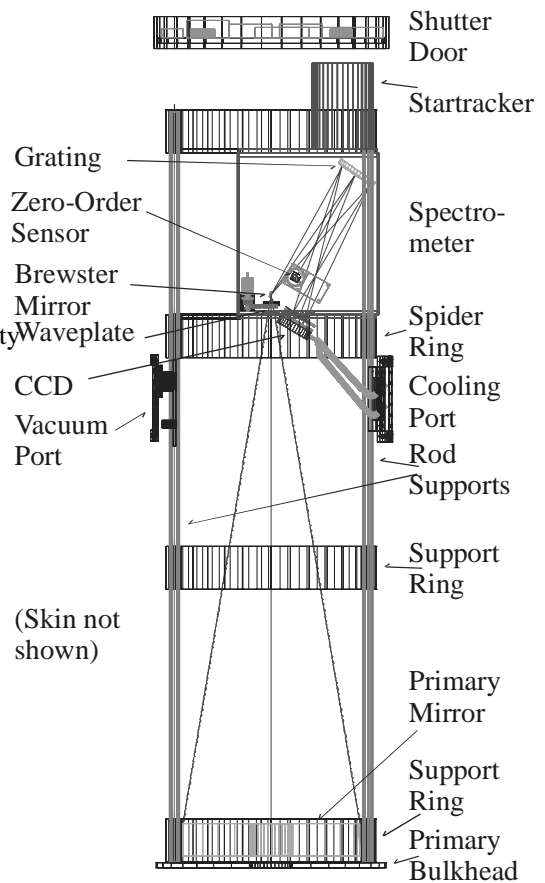


Figure 8 FUSP Telescope

CCD, cooled to about -65 °C by a Thermo-Electric Cooler.

The primary mirror and spectrometer coatings will be LiF overcoated Aluminum. The entire telescope section may be evacuated or backfilled with dry nitrogen, with the aperture sealed by a NASA standard vacuum door. This is desirable in order to preserve the delicate LiF coatings and to provide an FUV liveness test in the field.

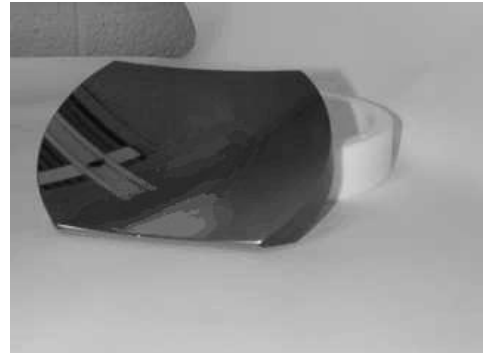
The polarimetric modulator is a 12 mm square, 1 mm thick stressed-LiF waveplate, mounted just before the focus. The



Figure 10 Diamond brewster mirror

angle. The materials requirement for Brewster reflection is an index of refraction greater than one. The greater the index of refraction, the higher the Brewster angle, and the higher the reflectivity at the Brewster angle. Diamond is the only known material to maintain  $n > 1.5$  down to 105 nm: in fact it remains above 3 for the entire FUSP range. The FUSP Brewster mirror (Figure 10) is a 0.5 mm thick CVD artificial diamond fabricated by Drukker International. Calculation of the polarization efficiency of a diamond mirror in an F/3.5 beam gives 60% at 105 nm, 85% at Ly $\alpha$ , and > 90% above 140 nm. The diamond mirror will be bonded to a substrate that is reflective in the visible so that a pointing monitor at the zero order of the spectrometer may aid in acquiring the target.

The dispersor is a 10 cm diameter spherical holographic grating (Figure 11) with a radius of curvature of 35 cm and a groove density of 1500 g/mm. It was fabricated by Jobin-Yvon. The spectrograph design uses aberration correction<sup>17</sup> to minimize coma and astigmatism. The mean rms width in the direction of dispersion is 27 microns. Combined with the rocket pointing blur, the resolution in the dispersion direction is 38 $\mu$  (1.6 pixels; 0.07 nm) giving R=1800 (165 km/s). Resolution perpendicular to the dispersion ranges from 2 – 30 pixels (8 – 120 arcsec).



**Figure 11** Aberration corrected Holographic Grating

In operation, the FUSP experiment timeline will consist of fairly short exposures, approximately 10 sec, on each waveplate position. The CCD readouts would be binned roughly 1x8 pixels (0.04 nm x 30 arcsec) to reduce the readout time to less than 1 second. The CCD will be operated shutterless: one half of the chip is masked off and the spectral data is rapidly shifted into this storage region and read out during the waveplate rotation. Like PFIS, eight images with equally-spaced waveplate angles from 11.25° to 90° will comprise a polarimetric measurement. This should give the highest possible precision achievable with a one beam device, better than 0.1%. The estimated system effective area will be 37 cm<sup>2</sup> at 120 nm, based on mirror efficiencies of 80%, obscuration 20%, brewster reflectivity 35%, grating efficiency 35%, actual LiF transmission, and detector quantum efficiency 35%. A 300 second exposure on a 0<sup>m</sup> (flat F $\lambda$ ) object will give ~ 2.5x10<sup>7</sup> ph/nm (0.06% polarimetric precision/0.1 nm) at 120 nm.

### 3.3 Scientific Programs/ Flights

Three separate diagnostics are to be tested in the FUSP flight series:

- Envelope dynamics through electron scattering competing with absorption lines
- Envelope physical state through polarization by Hydrogen Rayleigh scattering
- Envelope magnetic field through polarized resonance scattered lines and the Hanle Effect

Program	Target	m <sub>133</sub>	Exp(s)	$\Delta\lambda$ (nm)	%Err
Unpol	$\beta$ Tau	-0.5	50	1	0.03
Be	$\zeta$ Tau	-0.3	300	0.1	0.05
Hanle	$\zeta$ Ori	-2.5	200	0.1	0.02
Hanle	$\xi$ Per	1.0	150	0.1	0.1
IntBin	$\beta$ Lyr	2.	200	0.1	0.16
ISM	$\sigma$ Sco	-0.5	150	1	0.02

**Table 3** FUSP flight targets

In many objects several of these are expected to be important simultaneously. However, for simplicity, we will describe only the most important diagnostic with each object. Table 1 lists three candidate FUSP flights. Specific targets are shown together with the 133 nm magnitude, exposure time, required resolution, and the predicted precision, binning the data to that resolution. The total science exposure time for this payload is predicted to be 350 sec. The first flight is to be on the unpolarized standard  $\beta$  Tau, and the highly polarized Be star  $\zeta$  Tau. This will serve as a performance verification test against objects of known polarization, and will be a first exploration of the first two diagnostics. The second flight will be the first major test of the Hanle Effect magnetic field diagnostic, using the slow and rapid rotator O stars  $\zeta$  Ori and  $\xi$  Per. The third will probably target the interacting binary,  $\beta$  Lyr, and the interstellar polarization target,  $\sigma$  Sco.

## ACKNOWLEDGEMENTS

FUSP is supported by NAG5-5253.

## REFERENCES

1. N. Visvanathan, "Comparison of the optical spectrum of the filaments with the spectrum of the central region of M 82", *ApJ* **192**, pp 319–324, 1974.
2. J. Meaburn, R.D. Wolstencroft, and J.R. Walsh, "Echelle and spectropolarimetric observations of the Eta Carinae nebulosity", *A&A* **181**, pp 333–342, 1987.
3. K. Nordsieck, "New Circumstellar Magnetic Field Diagnostics", in *Magnetic fields across the Hertzsprung-Russell diagram*, ASP Conf. Ser. **248**, eds. G. Mathys, S.K. Solanki & D.T. Wickramasinghe (San Francisco: ASP), pp–607–616, 2001. (astro-ph/0106114)
4. D.A.H. Buckley, J.B. Hearnshaw, K.H. Nordsieck, and D. O'Donoghue, "Science with the Southern African Large Telescope (SALT)," in *Discoveries and Research Prospects from 6- to 10-Meter-Class Telescopes II. Proc SPIE*, **4834**, paper 34, 2002.
5. J.G. Meiring, D.A.H. Buckley, M. Lomberg, and R. Stobie, "Southern African Large Telescope (SALT) project: progress and status after 2 years," in *Large Ground-Based Telescopes, Proc SPIE*, **4837**, paper 3, 2002.
6. L.W. Ramsey, M.T. Adams, T.G. Barnes, J.A. Booth, M.E. Cornell, J.R. Fowler, N.I. Gaffney, J.W. Glaspey, J.M. Good, G.J. Hill, P.W. Kelton, V.L. Krabbendam, L. Long, P.J. MacQueen, F.B. Ray, R.L. Ricklefs, J. Sage, T.A. Sebring, W.J. Spiesman, and M. Steiner, "Early performance and present status of the Hobby-Eberly Telescope", in *Advanced Technology Optical/ IR Telescopes VI, Larry M. Stepp, Ed., Proc. SPIE*, **3352**, pp. 34–42, 1998.
7. E. B. Burgh, K. H. Nordsieck, H. A. Kobulnicky, T. B. Williams, D. O'Donoghue, M. P. Smith, and J. W. Percival, "The Prime Focus Imaging Spectrograph for the Southern African Large Telescope: Optical Design," in *Instrument Design and Performance for Optical/Infrared Ground-Based telescopes, Proc. SPIE*, **4841**, paper 164, 2002.
8. H.A. Kobulnicky, K.H. Nordsieck, E.B. Burgh, M.P. Smith, J.W. Percival, T.B. Williams, and D. O'Donoghue, "Prime Focus Imaging Spectrograph for the Southern African Large Telescope: Operational Modes," in *Instrument Design and Performance for Optical/Infrared Ground-Based telescopes, Proc. SPIE*, **4841**, paper 183, 2002.
9. R.W. Goodrich, M.H. Cohen, and A. Putney, "Spectropolarimetry. II: Circular polarization optics and techniques," *PubASP*, **107**, pp. 179–183, 1995.
10. W. Seifert, W. Mitsch, H. Nicklas, and G. Rupprecht, "FORS: a workhorse instrument for the ESO VLT," *Proc. SPIE*, **2198**, pp. 213–218, 1994.
11. N. Kashikawa, M. Inata, M. Iye, K. Kawabata, K. Okita, G. Kosugi, Y. Ohyama, T. Sasaki, K. Sekiguchi, T. Takata, Y. Shimizu, M. Yoshida, K. Aoki, Y. Saito, R. Asai, H. Taguchi, N. Ebizuka, T. Ozawa, and Y. Yadoumaru, "FOCAS: faint object camera and spectrograph for the Subaru Telescope," *Proc SPIE*, **4008**, pp. 104–113, 2000.
12. K. Serkowski, "Polarimeters for optical astronomy," in *Planets, Stars and Nebulae Studied with Photopolarimetry*, ed. T. Gehrels, pp. 135–174, University of Arizona, Tucson, 1974.
13. N. Thomas and J. Wolfe, "UV-shifted durable silver coating for astronomical mirrors," *Proc. SPIE*, **4003**, pp312–323, 2000.
14. S. Pancharatnam, "Achromatic combinations of birefringent plates," *Proc. Indian Acad. Sci.*, **A41**, pp. 137–144, 1955.
15. H. Metcalf and J.C. Baird, "Circular polarization of vacuum ultraviolet light by piezobirefringence," *Applied Optics* **5**, pp. 1407–1410, 1966.
16. C. Sanchez and M. Cardona, "Piezobirefringence in the vacuum ultraviolet: alkali halides and alkaline-earth fluorides," *Phys. Stat. Sol. (b)* **50**, pp. 293–304, 1972.
17. J.C. Green, E. Wilkinson and S.D. Friedman, "Design of the Far Ultraviolet Spectroscopic Explorer spectrograph," *Proc SPIE*, **2283**, pp. 12–19, 1994.